PREPRINT

tascc

TASCC-P-96-28

EXCLUSIVE MULTIDETECTION AND STUDY OF PROJECTILE BREAKUP AT 25 AND 35A MeV IN $^{24}Mg + ^{197}Au$ *

M. Samri†, L. Beaulieu, B. Djerroud‡, D. Doré§, R. Laforest, Y. Larochelle, J. Pouliot††, R. Roy and C. St-Pierre**

Laboratoire de physique nucléaire, Département de physique, Université Laval, Sainte-Foy, Québec, Canada G1K 7P4

G.C. Ball, A. Galindo-Uribarri, E. Hagberg and D. Horn

AECL, Chalk River Laboratories, Chalk River, ON, Canada K0J 1J0

* *Experiment performed at TASCC, AECL, Chalk River, Ontario, Canada K0J 1J0*

† *Correspondence to: M. Samri, Département de physique, Université Laval, Sainte-Foy, Québec, Canada G1K 7P4, Tel: (418) 656-2131 ext. 8919, Fax: (418) 656-2040, email: msamri@phy.ulaval.ca*

‡ *Present address: NSRL, University of Rochester, New York, USA*

§ *Present address: Institut de Physique Nucléaire, 91406 Orsay Cedex, France*

** *Present address: AECL, Chalk River Laboratories, Chalk River, Ontario, Canada K0J 1J0*

†† *Present address: Département de Radio-Oncologie, Hôtel-Dieu, 1 rue Collins, Québec, Canada G1R 4J1*

Submitted to Nucl. Phys. A

Physical and Environmental Sciences
Chalk River Laboratories
Chalk River, ON K0J 1J0 Canada

1996 August

Exclusive Multidetection and Study of Projectile Breakup at 25 and 35A MeV in $^{24}Mg + ^{197}Au$ *

M. Samri†, L. Beaulieu, B. Djerroud ‡ , D. Doré § R. Laforest **, Y. Larochelle, J. Pouliot††, R. Roy and C. St-Pierre.

Laboratoire de physique nucléaire, Département de physique, Université Laval, Sainte-Foy, Québec, Canada G1K 7P4.

G.C. Ball, A. Galindo-Uribarri, E. Hagberg and D. Horn.

AECL, Chalk River Laboratories, Chalk River, Ontario, Canada K0J 1J0.

---

*Experiment performed at TASCC, AECL, Chalk River, Ontario, Canada, K0J 1J0.

†Correspondence to: M. Samri, Département de physique, Université Laval, Sainte-Foy, Québec, Canada G1K 7P4. Tel: (418) 656-2131 ext(8919), Fax: (418) 656-2040, email: msamri@phy.ulaval.ca

‡Present address: NSRL, University of Rochester, New York, USA

§Present address: Institut de Physique Nucléaire, 91406 Orsay Cedex, France.

**Present address: AECL, Chalk River Laboratories, Chalk River, Ontario, Canada K0J 1J0.

††Present address: Département de Radio-Oncologie, Hôtel-Dieu, 1 rue Collins, Québec, Canada, G1R 4J1.

Abstract

The breakup of the projectile ^{24}Mg, excited in peripheral collisions on a gold target, has been investigated at 25 and 35A MeV with a large scintillation-detector array allowing exclusive measurements. Absolute breakup cross sections were deduced and the projectile-like nucleus velocity and excitation energy have been reconstructed. The excitation energy partition between the projectile and the target is found to lie between the limits of equal excitation energy sharing and equal temperature with some evolution from one limit to the other. The statistical nature of the decay mechanism is inferred from global variables. Small relative angle analysis is applied to the six-alpha exit channel and the corresponding data were found to be consistent with a sequential evaporation decay mechanism, with some contribution from sequential fission at higher excitation energies. The time scale involved in the breakup of ^{24}Mg projectiles into the 6α and the 5α+H+H channels has been investigated by examining distortions in the fragment velocity distributions due to the Coulomb field of the target. A decrease in the quasi-projectile lifetime is observed as the mean excitation energy increases from 3.4A to 4.5A MeV.

Keywords: Nuclear Reactions, $^{197}Au(^{24}Mg, X)$; E_{lab}= 25, 35A MeV; measured multiple projectile breakup, reconstructed excitation energy, deduced time scale, model calculations.

PACS number(s): 25.70 -z, 25.70 Lm

I. INTRODUCTION

A great effort, both experimental and theoretical, is being devoted to the study of the formation and dissociation of nuclear systems at high excitation energies produced in intermediate energy heavy-ion collisions. One of the challenging questions under investigation is the way in which the excited nuclei disintegrate. In central reactions, experimental results on multifragmentation are for some authors consistent with a sequential picture [1] and for others with a simultaneous one [2]. Recently, Durand et al. [3] have analyzed fragment correlation functions for the system Pb + Au at 29A MeV and have found what might be an evolution from a sequential to a simultaneous decay mechanism. Although central collisions are the most commonly employed reactions to produce highly excited systems, peripheral reactions have also been used successfully. Most of these latter experiments have involved nuclear reactions induced by light or medium-light projectiles such as ^{12}C, ^{16}O, ^{20}Ne, ^{24}Mg, ^{32}S,^{35}Cl, ^{40}Ca on various targets and have been performed with large-solid-angle multidetectors allowing nearly exclusive measurements [4–21]. Most of these studies have concluded that the decay mechanism is essentially of a statistical sequential nature. Recently, the authors of ref. [18] have studied the disintegration of ^{20}Ne projectiles at 40A MeV and have found evidence for a breakup mechanism consisting of a prompt step producing both stable and unstable particles followed by the sequential decay of the unstable species. Thus, it seems necessary to follow the evolution of the deexcitation mechanism over a wide range of the intermediate-energy domain with a specific projectile and, for a given incident beam energy, to also follow the deexcitation mechanism for the whole range of the measured excitation energies. A great help in such studies is the experimental determination of the time scale for breakup [14,17,18,22].

In this paper, we report on the breakup of ^{24}Mg at 25A and 35A MeV incident energy, excited in peripheral collisions on a gold target, into a large number of exit channels (some of them consisting of as many as 9 charged particles). The experiment has been performed with a large scintillator array that will be described in section II. The different breakup channels

and their charge distributions together with a comparison to the statistical models, GENEVE [23] and GEMINI [24] will be given in section III. Measured absolute breakup cross sections of the different breakup channels will be compared to the theoretical predictions of the above-cited models in section IV. Section V will deal with the quasi-projectile reconstruction, its excitation energy and the sharing of this quantity with that of the target. A statistical variable analysis in terms of the kinetic energy fraction will be given in section VI. Small-relative-angle analysis applied to the six-alpha exit channels will be presented in section VI together with theoretical predictions from a numerical code developed for sequential and multifragmentation decay by Randrup and López [25,26]. In the present work, the sequential decay calculations have been divided into a pure binary fission decay and an evaporative decay. Distortion effects due to the target Coulomb field, recently used to extract the lifetime of excited projectiles [14,22], will be exploited in section VII for the 6α and the 5αHH channels. A general discussion follows in section VIII and finally a conclusion will be drawn in section IX.

II. EXPERIMENTAL SETUP AND EVENT SELECTION

The experiment was performed with ^{24}Mg beams of E = 25 and 35A MeV energy provided by the Tandem Accelerator SuperConducting Cyclotron facility (TASCC) at Chalk River. These beams were directed onto a gold target of 2.9 mg/cm^2 areal density. Charged reaction products were detected by the CRL-Laval array composed of 80 scintillation counters mounted on five beam-centered rings, covering the whole azimuthal domain and located at average polar angles of 8^0, 13^0, 20^0, 29^0 and 40^0 with respect to the beam direction. Since the angular coverage in the array begins at 6.9^0 and the grazing angle in the laboratory frame is 11.6^0 at 25A MeV(8.0^0 at 35A MeV) for this reaction, this array is well suited to the study of peripheral reactions since most of the projectile-like fragments will be detected. The three inner rings are composed of fast-slow ΔE-E phoswich detectors [27] while rings 4 and 5 are composed of CsI(Tl) scintillators [28]. These two types of rings are located at 51.5

and 21 cm from the target position and cover solid angles of 0.51 and 1.37 sr, respectively. The energy thresholds range in the phoswich detectors from 7.5A MeV for protons and alpha particles, up to 19.5A MeV for $Z = 12$ ions. The threshold in the CsI detectors is about 2A MeV for $Z = 1, 2$ particles. Particle identification was achieved by comparing the results of two separate charge integration gates of the analog pulses, one short and one long. Elements were resolved according to their charge number up to $Z = 12$ in the phoswich detectors and up to $Z = 4$ in the CsI scintillators. In the CsI array we obtained isotope identification for hydrogen and helium. A typical fast-slow gate spectrum from the CsI's in the present experiment can be found in Ref. [29]. The data were recorded on an event-by-event basis with each detector contributing to the trigger. For each event, the measured quantities were the energy, angle and element number (and mass for $Z = 1, 2$ in the CsI detectors) of the reaction products. Some detector energy calibration point were obtained by elastically scattered protons off a gold target at 15 and 25 MeV and by secondary beams. The energy response in the CsI's was derived from the direct energy-to-light relation of Ref. [29] while the phoswich detectors was derived from the relation given in [30]. The energy calibration was accurate to about $\pm$ 5%.

In the off-line analysis, events corresponding to the multiple breakup of the projectile were selected by requiring, that the total detected charge in each event be equal to the charge of the projectile. Light particles evaporated by an excited target-like nucleus could potentially contribute to these events. To investigate this point, we have used the code GENEVE [23], whose main features will be outlined in section III, and have found that hydrogen and helium ions evaporated by a target-like nucleus are mainly produced with a low energy and do not pass the energy thresholds of the detectors. The contribution of preequilibrium particles was found to be negligible (less than 2%). The simulated GENEVE events that passed the geometrical and energy cuts of the detection apparatus correspond to a range of impact parameters peaking at about 9 fm which is characteristic a peripheral reactions. At this range of impact parameters, preequilibrium emission is negligible [31]. The measured differential cross sections for elements Z =1 up to Z =11 under the condition that

$\Sigma Z = 12$ decrease as a function of the detection angle, with slopes that become steeper as the fragment charge increases. Fig. 1 shows the velocity spectra at 25A MeV for elements from $Z = 1$ to $Z = 11$ under the condition $\Sigma Z = 12$. As the charge of the ejectiles increases, their distributions become narrower and approach the beam velocity. This, and the exponential falloff of the fragment's angular distributions is a characteristic pattern in projectile breakup and is generally taken as a signature of well characterized peripheral events [5]. This is also corroborated by the GENEVE simulations.

III. BREAKUP CHANNELS AND CHARGE DISTRIBUTIONS

A. Breakup channels

In the case of ^{24}Mg, there are 72 possible breakup channels into 2 to 9 charged particles. These channels, given in Table I, may be classified as a function of the charged-particle multiplicity or by their types. There are two main types of channels:

1. Channels with a PLF ($Z > 2$) accompanied by light charged particles ($Z = 1$ and/or $Z = 2$). The study of the excitation energy of these channels as a function of the projectile-like fragment mass was undertaken in Ref. [20] with the conclusion that light particle emission is statistical and comparable to the deexcitation of heavy and less excited nuclei.

2. Channels composed mostly of light charged particles ($Z = 1, 2$). These are of interest in the present study because of their high excitation energies and because the accurate energy calibration for light particles allows a precise reconstruction of the event. The channels 6α and 5αHH are studied below.

The indicated isotopic combinations in Table I is that leading to the least negative Q-value, denoted henceforth by Q_{least}. Within this attribution of Q-value, it is interesting to note that $Z = 2$ particles are always α particles. Experimental observations [32] and the present

GENEVE simulations show that $Z = 2$ particles are also alpha particles in about 90% of the cases. The indicated isotopic compositions in Table I, at least for channels with $Z = 2$ particles, are then expected to be the dominant deexcitation channels.

B. Charge distribution

The measured charge distributions, given the condition that $\Sigma Z = 12$ are shown in Fig. 2. Because of high probabilities for breakup into 2 or 3 charged particles, elements of charge 1, 2, 10, and 11 are produced with a high yield. An interesting systematic feature is the high yield of most alpha-cluster fragments relative to the yields of neighboring elements (i.e. the yield of oxygen is greater than those of nitrogen or fluorine). This most likely results from the alpha-structure of ^{24}Mg [33] that favors the emission of alpha and alpha-cluster fragments. The experimental charge distributions were compared to the theoretical predictions of two statistical codes: GEMINI and GENEVE.

In GENEVE simulations, the formation and deexcitation of the hot nuclei produced in the reaction are decoupled. The rates of neutron and proton preequilibrium emission are determined for each impact parameter by the overlap of the projectile and the target in coordinate and momentum spaces. For impact parameters lower than the value for which the pocket in the interacting potential disappears the dissipative phase is described by a fusion-like process. For larger impact parameters, a binary process is assumed in which the amount of dissipated energy and angular momentum is estimated in the framework of kinetic equations such as BUU or LV [34]. Hot nuclei are finally deexcited in a statistical approach by which a sequential binary decay is assumed and all channels from light-particle emission to symmetric fragmentation are included. For both codes the ouputs are the excitation energy and velocity of the projectile and of the target at the end of the excitation stage, and the characteristics (velocity, angle) of their decay products and of preequilibrium particles: a label is placed on each particle specifying its precursor source.

In the GEMINI calculations, the experimental excitation energy distribution corrected

for detection efficiency and the angular momentum of the decaying nucleus are used as input. The angular momentum of the ^{24}Mg nucleus was calculated by the reaction code TORINO [35] which takes into account the statistical exchange of nucleons between the two colliding nuclei and a deformation term arising from surface collective excitations. This calculation gives mean values of $6\hbar$ and $8\hbar$ with a variance of $2\hbar$ for the reactions at 25 and 35A MeV respectively. These mean values were calculated by giving to each value of angular momentum the experimental weight of the corresponding experimental excitation energy. An advantage of this procedure is that the calculated angular momentum is correlated to the experimental excitation energy.

The charge distributions simulated by the codes GENEVE and GEMINI are given in Fig. 2 where they are seen to reproduce the general shape of the experimental charge distribution with the following discrepancies:

1. The high yield of most alpha-cluster fragments with respect to the yields of neighboring elements is not reproduced by the simulations, since these calcultations do not take account of the nuclear structure of the decaying system. In the case of the nucleus ^{24}Mg, this structure is most likely to be of an alpha-cluster type [33].

2. The yields of charges $Z = 1$ and $Z = 9, 10, 11$, produced abundantly in the channels numbered in table I as 1, 7, 8 and 9 are not well reproduced by the GEMINI simulations.

3. Both calculations overestimate the production probability of charges 3 and 4 which are intermediate-mass fragments present in channels of high multiplicities and excitation energies (see the case of Li in the channels numbered 55 and 63 in Table I). In GEMINI calculations these channels have a high angular momentum (higher than $10\hbar$); the fact that the yield of the IMF is not well reproduced by the simulations may be an indication that the angular momentum of ^{24}Mg is not very high.

IV. BREAKUP CROSS SECTIONS

The experimental channel breakup cross sections corrected for detection efficiency are listed in Table I. The differential cross sections were used to evaluate the detection efficiency, taken as the ratio of the experimental yield of a particular element between 6^0 and 46^0 (the range covered by the multidetector) to the total yield from 0^0 to 180^0 [9]. The efficiency for detecting a particular breakup channel is taken to be the product of the individual efficiencies of the fragments composing that channel. This kind of evaluation may be justified empirically by the fact that the particle angular distributions have been demonstrated to be independent of the channels to which they belong [9]. The total breakup cross sections have been found to be 390 and 435 mb for the experiments at 25 and 35A MeV respectively, which values are about 10% of the estimated total reaction cross section [36]. The breakup into binary and ternary channels exhausts 90% of the breakup cross section (mainly the Na + H, Ne + He, Ne + H + H, F + He + H and O + He + He channels). Under the assumption of statistical decay, the graph representing the cross section as a function of the Q-value should exhibit an exponential decrease [9]. This trend has been observed in the breakup of ^{35}Cl at 30A MeV [16] and in ^{24}Mg at 70A MeV [37]. Yet, as the number of isotopic possibilities associated with each channel is high, the cross sections have large fluctuations around the exponential dependence. These fluctuations can be averaged by calculating the cross sections for each charged-particle multiplicity as a function of a mean Q-value calculated for each multiplicity. Such a calculation is given in Fig. 3. The mean Q-value was obtained by weighting the Q_{least} value attributed to the channel by the channel abundance for each multiplicity. For both incident beam energies, the exponential decrease of the cross section as a function of the Q-value is observed. This feature is well reproduced by the GENEVE simulations showing that the deexcitation of the magnesium projectiles proceeds mainly in a statistical way and is governed by the degrees of freedom available in the phase space.

V. EXCITATION ENERGY

A. Reconstruction of the quasi-projectile

The combined information on mass, angle and energy of the fragments allowed reconstruction of the velocity and excitation energy of the primary projectile-like nucleus (PLN). For the location of a hit on a detector we take a uniform random distribution over the detector area. The total reconstructed PLN velocity distribution, shown in Fig. 4, peaks at a value close to the beam velocity and is shifted to lower values as the multiplicity increases. Its mean value at 25A MeV falls from 93% to 80% of the beam velocity as the total multiplicity increases from 2 to 7. For the experiment at 35A MeV, the quasi-projectile velocity has a component towards lower velocities which might be due to contamination by particles evaporated from an excited quasi-target or an intermediate source. This component has been removed by requiring that the quasi-projectile velocity be greater than 75% of the beam velocity. Figure 4 also shows the quasi-projectile velocity predicted by the GENEVE code at the end of the excitation stage which has a shape and a mean value similar to the experimental distribution. Yet, the predicted velocity peaks closer to the beam velocity than the experimental velocity.

The particles' parallel and perpendicular velocities in the reconstructed PLN frame may be used to search for a possible contamination by particles from sources other than that of the PLN [13]. Fig. 5 shows a plot of the transverse versus parallel velocity components in the PLN rest frame of the $Z = 1$ and 2 particles. A depletion of counts can be seen around the center of mass of the parent nucleus showing the existence of a single source of emission of particles.

B. Quasiprojectile excitation energy

The PLN excitation energy is computed in the usual way [9] by summing the kinetic energies (in the rest frame of the PLN) of all fragments in a given channel, and then shifting

the computed value by the channel separation energy:

$$E^*_{qp} = \frac{1}{2}\sum_i M_i \mid \vec{V}_i - \vec{V}_{qp} \mid^2 - Q. \quad (1)$$

The mean channel excitation energies for both experiments, calculated with the appropriate Q_{least} value are given in Table I. The mean values are typically 20 MeV for binary channels but can reach high values (around 120 MeV) for high charged-particle multiplicities. For most channels, the mean excitation energies at 35A MeV are higher than those at 25A MeV which validates the kinematical reconstruction procedure. The rare exceptions (channels 15 and 17) are due to the presence of lithium which missed the CsI detectors in the 35A MeV experiment. The extracted excitation energies are found to be highly correlated to the charged-particle multiplicity in these detectors. Total excitation energy spectra including all channels are given in Fig. 6. We observe events with as high as 140 MeV and 175 MeV (5.8A MeV and 7.3A MeV) for the experiments at 25 and 35A MeV respectively. For the 35A MeV experiment, the contribution to the high-energy part is due mainly to newly opened channels (labels 58, 59, 61, 68 and 72 in Table I) which have a very high Q-value and require higher excitations. This suggests that despite the increase in beam energy, the maximum excitation energy in the ^{24}Mg nucleus has not been reached at 35A MeV. The experimental excitation distributions are compared in Fig. 6, to the predictions of the GENEVE calculations at the end of the first stage. The predicted distributions cover the same range as the experimental ones and have the same shape. The reaction code TORINO [35] also predicts quasi-projectile excitation energies ranging from 20 to 120 MeV and associates the higher values with medium impact parameters.

To evaluate the effect of the lack of isotopic resolution on the excitation energy determination, a second set of Q-values was used. In a first step, the excitation energy calculated with the Q_{least} value was used as input in a GEMINI simulation. A mean value of the separation energies (Q_{mean},) of all simulated and detected isotopic combinations for a given channel was calculated. The two sets of values, Q_{least} and Q_{mean}, are given in Table I. For low-multiplicity channels and for channels with alpha particles and alpha-cluster like frag-

ments, the Q_{mean} values are not much higher than the Q_{least} values. This may be understood by the fact that for these channels, the number of isotopic combinations is relatively small and also because $Z = 2$ particles are, for about 90% of the cases, alpha particles (Ref. [32] and the present simulations). For highly fragmented channels and for those channels containing $Z = 1$ particles, the discrepancy between the two sets of Q-values is more pronounced because of the many isotopic combinations involving hydrogen isotopes, and consequently there is a shift in the excitation energies of $(Q_{mean} - Q_{least}) \approx 10$ MeV of these channels. Nevertheless, the spectral shape of the excitation energy distribution is unchanged.

C. Excitation energy partition

The excitation energy partition between the projectile and the target can give some information on the degree of thermalization reached between the two partners in a nuclear reaction and is also important to theoretical models, which involve different assumptions for this sharing [38]. For small interaction times, thermal equilibrium may not be reached and the projectile and target will be on average excited equally due to the rapid exchange of nucleons. For longer interaction times, the projectile and the target may reach equilibrium and the ratio of the excitation energy of the target to the projectile will be in the ratio of their masses. This picture appropriate at low incident energy [39] seems also to be the case at higher incident energies [14,15,40,41]; yet the data in this higher energy domain are scarce and more experimental determinations of energy sharing are needed.

In this work, the target excitation energy E^*_{qt}, was computed under the assumption of two-body kinematics with conservation of momentum and energy, [9,42]

$$E^*_{qt} = E_i - K_{qp} - K_{qt} - E^*_{qp}, \tag{2}$$

with E_i being the initial incident energy and K_{qp}, K_{qt} the projectile and target kinetic energies. The latter quantity was computed from momentum conservation. The assumption of two-body kinematics is validated since, as shown above, the fragments originate from

an excited quasi-projectile and the contribution from an excited quasi-target is negligible because of the assymetry of the system (light projectile on a heavy target). The mean excitation energy values in the quasi-projectile and in the quasi-target for the most abundant channels of Table I are given in Fig. 7 for both experiments. The partition of excitation energy lies between the equal excitation sharing (EES) typical of a fast peripheral reaction and the equal temperature limit (ETL) characteristic of longer interaction times. A certain evolution can be seen from one limit to the other when the two beam energies are compared. This is illustrated in the figure by the channels joined by arrows for the two experiments. This trend is not due to our method of calculating the target excitation energy and is validated by GENEVE simulations. In these simulations, we have calculated the predicted ratio (at the end of the excitation stage) of the target and projectile excitation energies and compared it to that obtained from the reconstructed projectile excitation energy (calculated from the individual particles' velocities) and from the target excitation energy (calculated in the same way as in the experiment). The two ratios were found identical, showing that the evolution of this ratio from one limit (EES) to the other (ETL) cannot be attributed to the reconstruction procedure.

The effect of not detecting the neutrons must also be examined. The mean neutron multiplicity associated with channels of a given charged-particle multiplicity has been calculated with the code GENEVE. This number is found to vary from 0.2 to 1 as the charged-particle multiplicity increases from 2 to 7. Moreover, for most channels of high statistics (those containing Z=2 particles), the number of associated neutrons is low. In the simulation the mean energy carried out by the neutrons associated with each channel is at most 10 MeV and could not account of the observed evolution from the EES to the ETL limit.

VI. DEEXCITATION MECHANISM

A. Kinetic energy fraction

A new signature [43] of statistical decay has been derived from the kinetic energy fraction R given by

$$R = \frac{\sum E_{kin}}{(\sum E_{kin} + Q_o)}. \tag{3}$$

In the case of relatively low Coulomb barriers for emission, which is the case in the ^{24}Mg nucleus, the mean kinetic energy is equal to twice the temperature. Assuming that the final state level density is a continuous linear function of Q_o values, one also obtains that $< Q_o >= 2T$ [43]. The mean value of R is then equal to 0.5 and is independent of excitation energy. Another way to look at this ratio is to plot the mean excitation energy as a function of the channel Q-value which should then have a slope equal to 2. Figure 8 gives such a plot for the experiments at 25 and 35A MeV. The experimental points fall along the lines which show straight line fits to the data with slopes of 1.9 and 2.2 for the experiments at 25 and 35A MeV respectively. A constant ratio is observed for both beam energies over a large range of excitation energies indicating that the deexcitation mechanism is mainly statistical.

B. Small-relative-angle analysis

To further investigate the decay mechanism, we have constructed experimental relative angles between the alpha particles for the six-alpha channel and compared those angles to the predictions of the code SOS [25,26] developed to simulate sequential and simultaneous multifragmentation. In the sequential simulations, the fragments are emitted without correlation by a single equilibrated source with an excitation energy taken from the experimental distribution. The system undergoes successive splittings and the decay chain stops when the excitation energy is insufficient for further fragmentation. For each sequential event, we construct the corresponding simultaneous event which has the same number of fragment

and the same total energy. The fragments are gathered randomly in a sphere of a radius twice that of the magnesium nucleus and then expanded under the influence of Coulomb repulsion until asymptotic velocities are reached.

Two kinds of sequential events were simulated. Firstly, alpha particles were produced by all possible binary fission channels such as $^{24}Mg \Longrightarrow {}^{12}C + {}^{12}C$, $^{24}Mg \Longrightarrow {}^{16}O + {}^{8}Be$ or $^{24}Mg \Longrightarrow {}^{20}Ne + {}^{4}He$. Secondly, only alpha particles sequentially evaporated from ^{24}Mg (forming successively ^{20}Ne, ^{16}O, ^{12}C, ^{8}Be and 2 ^{4}He) were considered. We label the former sequential fission (SF) and the latter sequential evaporation (SE) in accordance with the nomenclature used in Ref. [44]. The simulated events were filtered through the geometrical and energy cuts of the experimental data. The sequential and simultaneous multifragmentation decays occur with different time scales. In the former, the time intervals between successive splittings are so long that any space-time correlation between emitted fragments is weak, while for the latter, fragments are emitted promptly and therefore experience a strong mutual Coulomb repulsion. In this case small relative angles will be suppressed. Relative angles between all pairs of alpha particles have been constructed and compared to the SOS (sequential fission, sequential evaporation and prompt) predictions in Ref. [19]. It has been found that the sequential evaporation simulation best reproduces the experimental data. Yet, in the region of small relative angles, both the sequential evaporation and sequential fission simulations are in agreement with the experimental data.

In order to look for a contribution of the sequential fission which should be important at higher excitations, the present study considers only the two smallest angles amongst the 15 pairs of angles. Figure 9 shows the distribution of these angles for the lowest and highest part of the excitation energy distributions at 25A MeV (left) and 35A MeV (right). For the lowest excitations, both the SF and SE simulations have the same shape and mean value as the experimental distribution. On the other hand, at higher excitations, the two simulated distributions are quite different (middle part of Fig. 9) and neither of them reproduces the experimental distribution. In order to reproduce the experimental distribution at higher excitations, contributions of about 30-40% of the SF mechanism and 60-70% of the SE

mechanism have to be used (bottom part of Fig. 9). It is interesting to note that while the combination of the two sequential paths reproduces the shape of the minimum angles at 25A MeV, the agreement is not as good at 35A MeV, and a certain contribution from the prompt decay may be needed in this case.

VII. QUASIPROJECTILE LIFETIME

The analysis of the preceding section gives qualitative information about the reaction mechanism but quantitative information is also needed. This can be obtained by determining the time scale involved in projectile breakup. In central collisions, time information is usually extracted either via particle correlation function based on the intensity interferometry method [45]: in projectile breakup experiments new methods [14,17,18,22,46] based on the target proximity effect [47] have been developed. These methods depend on the influence of the target Coulomb field on the final velocities of the fragments, and allow time determination with the help of event simulation.

The method [14,22] used in this study consists in simulating a series of velocity distributions as a function of the lifetime τ of the decaying ^{24}Mg nucleus, and in using the simulated final fragment velocities to construct a normalized velocity tensor

$$V_{ij} = \frac{1}{MN} \sum_{n=1}^{MN} (v_i^{(n)} - \overline{v}_i)(v_j^{(n)} - \overline{v}_j), \tag{4}$$

where $\overline{v}_i = \sum_{n=1}^{MN} v_i^{(n)}/MN$, with N, the total number of events and M, the multiplicity of each event. The indices i and j refer to different space fixed axes. The ordered ($q_1 \leq q_2 \leq q_3$) and normalized eigenvalues ($Q_i = q_i^2 / \sum_{j=1}^{3} q_j^2$) of this tensor yield the total coplanarity given by $C_T = \frac{\sqrt{3}}{2}(Q_2 - Q_1)$ [48,49]. The evolution of C_T as a function of τ is mapped out by several calculations assuming different values of τ. The experimental lifetime is obtained as the intersection of the experimental total coplanarity with that simulated. In the simulations, the initial relative position and momentum of the projectile and the target are calculated with the reaction code TORINO [35]. The sequential disintegration of ^{24}Mg is then followed

from the time $t = 0$ (set at the distance of closest approach) until all particles are emitted. At each stage of the decay chain, the position and the velocity of all particles are initially generated randomly in such a way as to conserve the linear momentum and position of the center of mass of the target and the projectile, and at later times, of the target and the fragments of the projectile. As we do not know how the lifetime is changing along a decay chain, we assumed an exponential decay law and the same decay constant for all decay steps. At each step, the lifetime is randomly chosen in this exponential distribution by the Monte-Carlo method. These assumption do not affect significantly the properties of the velocity tensor V_{ij} as these rely mainly upon the earliest emissions which carry away large amounts of excitation and angular momentum.

For each channel, two sets of simulations were performed corresponding to angular moment of $4\hbar$ and $8\hbar$ respectively. The code used in this work is that of Ref. [44]. The simulated events were filtered through the geometrical and energy cuts of the detection apparatus and a value of the total coplanarity was extracted for each value of τ. The excitation energy was obtained by summing the kinetic energies in the center of mass of the fragments and adding the separation energy for the reaction channel. This method has been applied to the 6α breakup at 25 and 35A MeV and to the 5αHH breakup at 25A MeV where the mean excitation energies are 80, 95 and 108 MeV respectively as given by Table I. In the case of the 5αHH channel, where mass resolution for hydrogen ions is achieved in the CsI detectors, the analysis is restricted to events where at least one proton is detected in those detectors ($24^0 \leq \theta \leq 46^0$). In this way, we select events (among which 8% are fully mass resolved 5αpp) with high excitation energy, since this quantity is found to be correlated with the charged-particle multiplicity in the CsI detectors.

The results for these channels, shown in Fig. 10, display the same smooth monotonic decrease of the total coplanarity as a function of the time delay observed in previous work [22,14]. The time delays corresponding to the experimental total coplanarities are approximately $(5.1 - 6.8) \times 10^{-22}$ s, $(4.7 - 6.8) \times 10^{-22}$ s and $(3.0 - 5.9) \times 10^{-22}$ s for the 6α channel at 25A MeV and 35A MeV and 5αHH at 25A MeV, respectively .

The lifetimes of the quasi-projectile are given in Table II as a function of the excitation energy per nucleon of the corresponding channel and for the two limiting cases of the assumed angular momenta. These lifetimes are dependent on the assumed angular momenta. The $4\hbar$ value does not seem very realistic since such small values are usually reported for lighter nuclei (such as oxygen at 25A MeV for which a value of $5\hbar$ has been suggested in Ref. [44]). In the case of ^{40}Ca, a value of $12\hbar$ has been reported at 35A MeV in a comparable excitation energy range [12]. Moreover the value of $4\hbar$ for the ^{24}Mg nucleus represents only 25% of the maximum value predicted by the systematics of ref. [50]. Of the two values of the angular momenta used in the simulations, the higher should be more realistic. Consequently, the lifetimes of the quasi-projectile at the different excitation energies should be closer to the values corresponding to the $8\hbar$ simulations.

VIII. DISCUSSION

The lifetimes of the quasi-projectile in the six-alpha channel decay are in agreement with low-energy statistical extrapolated times ($(5.4-6)\times 10^{-22}s$) [51]. These lifetimes are characteristic of statistical sequential decay and corroborate the results obtained with the small-relative-angle analysis of the present study and with results obtained previously [19,52]. In the case of the 5αHH channel, the deduced lifetime is smaller than the extrapolated statistical time ($4.7\times 10^{-22}s$) [51] and approaches thermalization times obtained in Ref. [53,54]. A short lifetime for the 5αHH channel ($3\times 10^{-22}s$) has been obtained in a preceding study [21] by a different method which used the velocity shift in the proton longitudinal velocity due to the Coulomb field of the target [17]. This method was originally applied to the same 5αHH channel at 60A MeV [17] and a lifetime of $3\times 10^{-22}s$ was reported. The authors of ref. [17] have also measured correlation functions between protons and other fragments and found that contributions from resonant states are very low, showing that protons should not be emitted by these intermediate states which have long lifetimes but are produced in a more prompt way. Short lifetimes were reported in other projectile studies

and were associated with a sequential decay mechanism. This is the case for the breakup of ^{16}O into four alpha particles at 25A MeV for which a lifetime of the order of $10^{-22}s$ was reported. Yet in the same study a sequential decay mechanism was inferred from relative-angle analysis. For the same nucleus but at 94A MeV, the authors of Ref. [14] have reported a lifetime much shorter ($(2-3)\times 10^{-22}s$), and have reproduced their data with sequential decay calculations. In other works, the observation of short lifetimes in the breakup of ^{24}Mg [17] and ^{20}Ne [18] has been associated to a prompt+sequential decay mechanism.

In order to understand the significance of the short lifetime determined in the present study, one should not consider it as an isolated measurement rather it should be considered in conjunction with the other values. With assuming an angular momentum value close to $8\hbar$, which is a realistic assumption, the lifetimes decrease withincreasing excitation energy per nucleon as shown in Table II. This decrease is observed for a given channel at different incident beam energies and for two different channels at the same beam energy. Considering the short lifetime which is smaller than the extrapolated statistical value and together with the fact that lifetimes decrease with the excitation energy suggests an evolution in the reaction mechanism. A purely sequential or a completely instantaneous multifragmentation of ^{24}Mg into the 5αHH channel are two extremes that are unlikely to occur. A more realistic image of the disintegration decay would be that of a breakup intermediate between these two extremes. An important task will be to evaluate quantitatively the relative importance of the two extremes. Concerning the breakup of ^{24}Mg, a candidate channel is the 8-fold channel consisting of 4 alpha particles and 4 protons in which the mean excitation energy per nucleon is as high as 6.5A MeV.

IX. CONCLUSION

The breakup of ^{24}Mg excited in peripheral collisions on a gold target has been studied at 25 and 35A MeV with a large multidetector array allowing exclusive measurements. Highly fragmented channels were observed corresponding to highly excited projectile-like nuclei.

The absolute cross sections of a large number of exit channels were measured and found to be correlated to the separation energies. These are well reproduced by statistical model calculations. Global variable analysis in terms of the kinetic energy fraction have shown that the decay mechanism is mainly statistical. The excitation energies of the projectile and of the target have been reconstructed and the energy partition is found to evolve smoothly between the limits of equal excitation energy sharing and equal temperature. Small-relative-angle analysis has been applied to the six-alpha channel and the corresponding experimental data are found to be consistent with a sequential evaporation mechanism with a contribution of sequential fission towards higher excitations. Distortion effects due to the target Coulomb field were exploited for the 6α and the 5αHH channels to deduce the lifetime of the quasi-projectile. A decrease in the emission times is found when the excitation energy per nucleon increases from 3.4 to 4.5A MeV. Thus, the smallest-relative-angle analysis and the observation of lifetime shorter than typical statistical times suggest an evolution in the reaction mechanism from sequential toward prompt decay.

ACKNOWLEDGMENTS

This work has been supported in part by NSERC (Canada). We are very grateful to Professor R.J. Charity and Dr. J.P. Wieleczko for supplying the codes used in this work.

REFERENCES

[1] P.R. Chomaz et al., Nucl. Phys. **A551**, 508 (1993).

[2] O. Lopez et al., Phys. Lett. **B315**, 34 (1993).

[3] D. Durand et al., Phys. Lett. **B345**, 397 (1995).

[4] S.B. Gazes et al., 712 Phys. Rev. C **38**, 712 (1988).

[5] C. Pruneau et al., Nucl. Phys. **A500**, 168 (1989).

[6] J. Pouliot et al., Phys. Lett. **B223**, 16 (1989).

[7] K.A. Griffionen et al., Phys. Rev. C **40**, 1647 (1989).

[8] R. Wada et al., Phys. Rev. C **39**, 497 (1989).

[9] J. Pouliot et al., Phys. Rev. C **43**, 735 (1991).

[10] D. Doré et al., Nucl. Phys. **A545**, 363 (1992).

[11] C. Schwartz et al., Z. Phys. **A 345**, 29 (1993).

[12] A. Lleres et al., Phys. Rev. C **48**, 2753 (1993).

[13] P. Désesquelles et al., Phys. Rev. C **48**, 1828 (1993).

[14] A. Badalà et al., Phys. Rev. C **48**, 633 (1993).

[15] R. Laforest et al., Nucl. Phys. **A568**, 350 (1994).

[16] L. Beaulieu et al., Nucl. Phys. **A580**, 81 (1994).

[17] R.J. Charity et al., Phys. Lett. **B323**, 113 (1994).

[18] R.J. Charity et al., Phys. Rev. C **52**, 3126 (1995).

[19] M. Samri et al., Nucl. Phys. **A583**, 427 (1995).

[20] L. Beaulieu et al., Phys. Rev. C **51**, 3492 (1995).

[21] M. Samri et al., Phys. Lett. **B373**, 40 (1996).

[22] J. P. Bondorf et al., Phys. Rev. **C 46**, 374 (1992).

[23] J.P. Wieleczko et al., Proceedings of the 2^{nd} TAPS Workshop, Guardamar, Spain, ed. by Diaz, Martinez and Schutz, World Scientific, p 145 (1993).

[24] R.J. Charity et al., Nucl. Phys. **A483**, 371 (1988).

[25] J.A. Lopez and J. Randrup, Nucl. Phys. **A491** , 477 (1989).

[26] J.A. Lopez and J. Randrup, Comp. Phys. Comm. **70**, 92 (1992).

[27] C. Pruneau et al., Nucl. Inst. and Meth. **A297**, 404 (1990).

[28] M. Gourde, Ms. Thesis, Université Laval , (1993) (unpublished).

[29] Y. Larochelle et al., Nucl. Instr. and Meth. in Phys. Res. **A348**, 167 (1994).

[30] J. Pouliot et al., Nucl. Instr. and Meth. **A270**, 69 (1988).

[31] C. Cerruti et al., Nucl. Phys. **A492**, 322 (1989).

[32] D. Doré, Ph.D. Thesis, Université Laval , (1994) (unpublished).

[33] A.H. Wuosmaa et al., Phys. Rev. Lett **68**, 185 (1992).

[34] G.F. Bertsch, Phys. Rev. **C 29**, 675 (1984).
G. Grégoire et al., Nucl. Phys. **A465**, 317 (1987).

[35] C.H. Dasso and G. Pollarolo, Comp. Phys. Comm. **50**, 341 (1988).

[36] W.W. Wilke et al., Atom. and Nucl. Data. Tab. **25**, 389 (1980).

[37] D. Doré et al., Phys. Lett. **B323**, 103 (1994).

[38] B. Borderie et al., Ann. Phys. Fr. **15**, 287 (1990).

[39] J. Tõke and W.U. Schröder, Ann. Rev. Nucl. Part. Sci. **42**, 401 (1992).

[40] B. Borderie et al., Z. Phys. **A338**, 369 (1991).

[41] J. Pouliot et al., Phys. Lett. **B263**, 18 (1991).

[42] H.R. Schmidt et al., Phys. Lett. **B180**, 9 (1986).

[43] D. Horn et al., Proceedings of the Workshop on Heavy-Ion Fusion, Padua, Italy, 1994 ed. A.M. Stefanini, G. Nebbia, S. Lunardi, G.Montagnoli and A. Vitturi, World Scientific, p. 208 (1994).

[44] R.J. Charity et al., Phys. Rev. **C 46** , 1951 (1992).

[45] D.H. Boal and C.K. Gelbke, Rev. of Mod. Phys. **62**, 553 (1990).

[46] K. Ieki et al., Phys. Rev. Lett. **70**, 730 (1993).

[47] D.V. Harrach et al., Phys. Rev. Lett. **48**, 1093 (1982).

[48] M. Gyulassy et al., Phys. Lett. **B110**, 185 (1982).

[49] G. Fai and J. Randrup, Nucl. Phys. **A 404**, 551 (1983).

[50] R. Schmidt and H. Lutz, Phys. Rev. **A 45**, 7981 (1992).

[51] D. Shapira et al., Phys. Rev. **C 10**, 1063 (1974).

[52] R. Roy et al., Proceedings of the XXXIII International Winter Meeting on Nuclear Physics, Bormio (Italy), 1995 January 23-27 Ed. I. Iori, Dept. Physics, Univ. Milano, (1995).

[53] B. Borderie, Ann. Phys. Fr. **17**, 349 (1992).

[54] D. Durand and B. Tamain, in École Joliot-Curie de Physique Nucléaire, IN2P3, 135 (1993).

TABLES

TABLE I. ^{24}Mg breakup channels and the corresponding separation energies. Q_{least} is the least negative Q-value for all isotopic combinations of the detected elements and Q_{mean} is the mean of the Q-values of all the simulated (GEMINI) and detected isotopic combinations for a given channel. The isotopic combination given in column one is that leading to Q_{least}. Also given are the experimental mean excitation energies and the absolute breakup cross sections.

TABLE II. Quasiprojectile lifetime for the 6α and 5αHH channels in the reaction ^{24}Mg + ^{197}Au at 25 and 35A MeV as a function of the channel excitation energy per nucleon and for the two extreme values of the assumed angular momenta.

FIGURES

FIG. 1. Velocity spectra at 25A MeV for elements Z =1 up to Z =11 recorded in the phoswich detectors from 6^0 to 24^0 . Spectra for ^{2}H and ^{3}H were obtained with the CsI(Tl) detectors from 24^0 to 46^0. The arrows indicate the beam velocity.

FIG. 2. Experimental and simulated charge distributions with the codes GEMINI and GENEVE.

FIG. 3. Breakup cross sections in the reaction ^{24}Mg + ^{197}Au at 25 and 35A MeV for the different charged-particle multiplicities plotted as a function of the Q-value. The predictions of the codes GEMINI and GENEVE are also given.

FIG. 4. Experimental reconstructed PLN velocity distribution under the condition Σ Z = 12 and comparison to the predictions of the code GENEVE. Left arrows indicate the reaction c.m. velocity and right arrows indicate the beam velocity.

FIG. 5. Distributions of the experimental parallel velocity component versus the perpendicular velocity component for $Z = 1, 2$ particles under the condition Σ Z = 12

FIG. 6. Reconstructed quasi-projectile total excitation energy spectrum and comparison to the predictions of the code GENEVE.

FIG. 7. Mean target excitation energy vs. projectile exitation energy for the most abundant channels listed in Table I. Triangle and dot symbols refer to the experiments at 25 and 35A MeV respectively. Arrows join some specific channels labelled by their attributed number in Table I. The lines of equal temperature limit (ETL) and equal excitation sharing (EES) are indicated.

FIG. 8. Mean excitation energy for each channel as a function of its Q-value. The lines represent linear fits to the data.

FIG. 9. Experimental and simulated smallest-relative-angle distributions for the six-alpha exit channel in the 25A MeV (left) and 35A MeV (right) experiments. The experimental data are given by dots and the simulations by solid histograms (sequential evaporation), dotted histograms (sequential fission) and hatched histograms (simultaneous multifragmentation). All distributions are normalized to the same total number of counts.

FIG. 10. The curves represent the simulated total coplanarity values as a function of the time delay in the breakup of ^{24}Mg into six alpha particles at 25A MeV (top), at 35A MeV (middle) and into 5α + H + H particles at 25A MeV (bottom). The full and dashed curves correspond to angular momenta of $4\hbar$ and $8\hbar$ for the decaying ^{24}Mg nucleus, respectively. The experimental coplanarity values for each channel are indicated with horizontal bars.

Channel	Channel composition	Q_{least} [MeV]	Q_{mean} [MeV]	E= 25A MeV		E= 35A MeV	
				σ [mb]	$< E^* >$ [MeV]	σ [mb]	$< E^* >$ [MeV]
1	^{23}Na + p	-11.69	-15.83	130.99	17	186.96	19
2	^{20}Ne + α	-9.31	-9.88	94.33	19	97.63	21
3	^{19}F + ^{5}Li	-24.12	-27.33	1.24	39	0.48	43
4	^{16}O + ^{8}Be	-14.14	-27.02	0.57	30	0.64	30
5	^{15}N + ^{9}B	-26.45	-28.51	0.26	41	0.25	47
6	^{12}C + ^{12}C	-13.93	-19.21	0.58	25	0.55	28
7	^{22}Ne + 2p	-20.48	-31.24	17.37	32	40.56	37
8	^{19}F + α + p	-22.16	-28.02	18.09	40	24.04	46
9	^{16}O + ^{7}Li + p	-31.39	-36.69	0.83	56	0.78	64
10	^{16}O + 2α	-14.04	-15.30	27.54	33	23.38	38
11	^{15}N + ^{8}Be + p	-26.26	-35.38	0.31	50	0.48	58
12	^{15}N + ^{5}Li + α	-28.14	-34.20	1.34	55	0.76	58
13	^{12}C + ^{11}B + p	-29.89	-36.91	0.44	50	0.58	61
14	^{12}C + ^{8}Be + α	-21.30	-33.32	0.74	47	0.69	54
15	^{14}C + 2^{5}Li	-40.31	-47.52	0.05	72	0.01	59
16	^{9}B + ^{11}B + α	-37.44	-39.62	0.18	62	0.12	69
17	^{11}B + ^{8}Be + ^{5}Li	-39.22	-51.54	0.02	68	0.01	66
18	3^{8}Be	-28.76	-	0.00	-	0.00	-
19	^{21}F + 3p	-35.75	-50.04	0.48	57	2.25	73
20	^{18}O + α + 2p	-30.15	-38.64	4.28	55	14.16	69
21	^{15}N + ^{7}Li+ 2p	-43.52	-53.21	0.11	75	0.30	88
22	^{15}N + 2α + p	-26.17	-32.83	6.95	54	12.52	67
23	^{14}C + ^{8}Be + 2p	-36.47	-48.00	0.07	66	0.31	80
24	^{14}C + ^{5}Li + α + p	-38.34	-43.53	0.93	73	0.96	82

25	$^{12}C + 3\alpha$	-21.21	-23.86	5.41	53	5.01	63
26	$2^{11}B + 2p$	-45.84	-56.16	0.02	75	0.06	91
27	$^{11}B + {}^{8}Be + \alpha + p$	-37.25	-48.43	0.20	71	0.31	82
28	$^{11}B + {}^{5}Li + {}^{7}Li + p$	-56.48	-62.41	0.01	100	0.01	112
29	$^{11}B + {}^{5}Li + 2\alpha$	-39.13	-50.91	0.44	77	0.22	82
30	$2^{8}Be + {}^{7}Li + p$	-46.01	-	0.00	-	0.01	-
31	$2^{8}Be + 2\alpha$	-28.66	-42.40	0.11	66	0.10	76
32	$^{8}Be + {}^{5}Li + {}^{7}Li + \alpha$	-47.89	-55.20	0.02	94	0.01	82
33	$2^{5}Li + 2\ {}^{7}Li$	-67.11	-	0.00	-	0.00	-
34	$^{20}O + 4p$	-46.89	-58.73	0.05	78	0.72	98
35	$^{15}N + \alpha + 2p + t$	-45.99	-56.11	0.26	81	2.97	101
36	$^{14}C + {}^{7}Li + 3p$	-53.73	-64.02	0.02	100	0.13	109
37	$^{14}C + 2\alpha + 2p$	-36.38	-46.74	1.66	74	7.07	92
38	$^{11}B + {}^{8}Be + 2p + t$	-57.07	-69.97	0.01	90	0.05	122
39	$^{11}B + {}^{7}Li + \alpha + 2p$	-54.51	-64.33	0.05	101	0.22	116
40	$^{11}B + 3\alpha + p$	-37.16	-46.10	0.97	78	2.04	94
41	$2\ {}^{8}Be + \alpha + p + t$	-48.48	-57.15	0.02	92	0.05	105
42	$^{8}Be + 2^{7}Li + 2p$	-63.27	-	0.00	-	0.00	-
43	$^{8}Be + {}^{7}Li + 2\alpha + p$	-45.92	-52.38	0.17	95	0.31	104
44	$^{8}Be + 4\alpha$	-28.57	-31.86	0.47	73	0.57	86
45	$^{5}Li + 2^{7}Li + \alpha + p$	-65.14	-76.02	0.01	134	0.01	114
46	$^{5}Li + {}^{7}Li + 3\alpha$	-47.79	-47.79	0.14	101	0.09	104
47	$^{15}N + 3p + 2t$	-65.80	-	0.00	-	0.06	133
48	$^{14}C + \alpha + 3p + t$	-56.19	-69.73	0.01	101	0.92	127
49	$^{11}B + {}^{7}Li + 3p + t$	-74.32	-	0.00	-	0.01	161
50	$^{11}B + 2\alpha + 2p + t$	-56.98	-67.12	0.07	105	0.86	131
51	$2\ {}^{8}Be + 2p + 2t$	-68.29	-	0.00	-	0.00	-

52	$^{8}Be + {}^{7}Li + \alpha + 2p + t$	-65.73	-75.83	0.01	125	0.08	140
53	$^{8}Be + 3\alpha + p + t$	-48.39	-55.78	0.15	100	1.04	121
54	$3^{7}Li + 3p$	-80.52	-	0.00	-	0.00	-
55	$2^{7}Li + 2\alpha + 2p$	-63.17	-71.99	0.02	129	0.10	132
56	$^{7}Li + 4\alpha + p$	-45.83	-50.72	0.32	103	0.84	115
57	6α	-28.48	-40.69	0.42	80	0.79	95
58	$^{14}C + 4p + 2t$	-76.01	-	0.00	-	0.01	157
59	$^{11}B + \alpha + 3p + 2t$	-76.79	-	0.00	-	0.05	169
60	$^{8}Be + {}^{7}Li + 3p + 2t$	-85.55	-	0.00	-	0.00	-
61	$^{8}Be + 2\alpha + 2p + 2t$	-68.20	-	0.00	-	0.19	156
62	$2^{7}Li + \alpha + 3p + t$	-82.99	-	0.00	-	0.00	-
63	$^{7}Li + 3\alpha + 2p + t$	-65.64	-77.57	0.02	129	0.50	150
64	$5\alpha + p + t$	-48.29	-62.02	0.18	105	1.75	130
65	$^{11}B + 4p + 3t$	-96.60	-	0.00	-	0.00	-
66	$^{8}Be + \alpha + 3p + 3t$	-88.01	-	0.00	-	0.02	175
67	$2^{7}Li + 4p + 2t$	-102.80	-	0.00	-	0.00	-
68	$^{7}Li + 2\alpha + 3p + 2t$	-85.46	-	0.00	-	0.04	179
69	$4\alpha + 2p + 2t$	-68.11	-82.04	0.01	131	0.40	165
70	$^{8}Be + 5p + 4t$	-107.83	-	0.00	-	0.00	-
71	$^{7}Li + \alpha + 4p + 3t$	-105.27	-	0.00	-	0.00	-
72	$3\alpha + 3p + 3t$	-87.92	-	0.00	-	0.04	192

TABLE I. M. Samri et al.

Channel	ϵ^* (A MeV)	τ (10^{-22}s)	
		J=8$\hbar$	J=4$\hbar$
6α at 25A MeV	3.4	5.1	6.8
6α at 35A MeV	4.0	4.7	6.8
5αHH at 25A MeV	4.5	3.0	5.9

TABLE II M.Samri et al.,

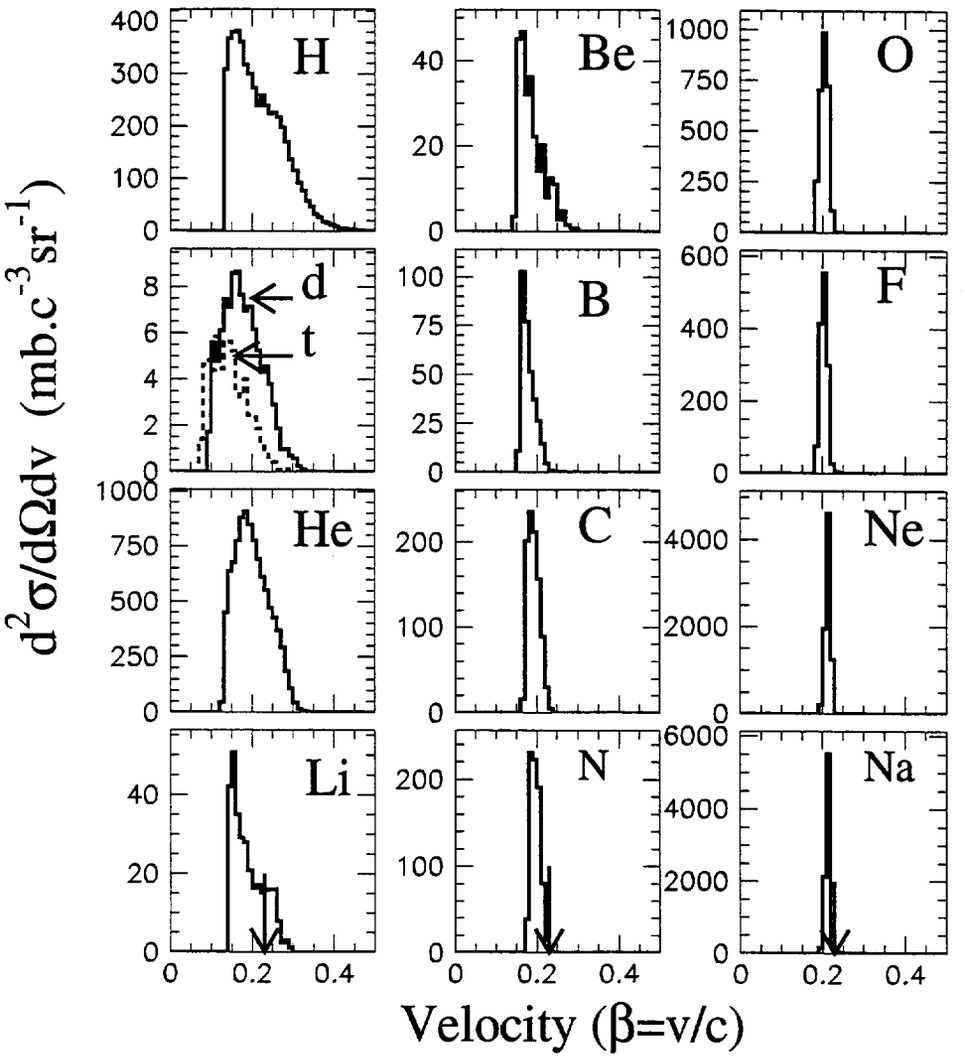

FIG. 1. M. Samri et al.

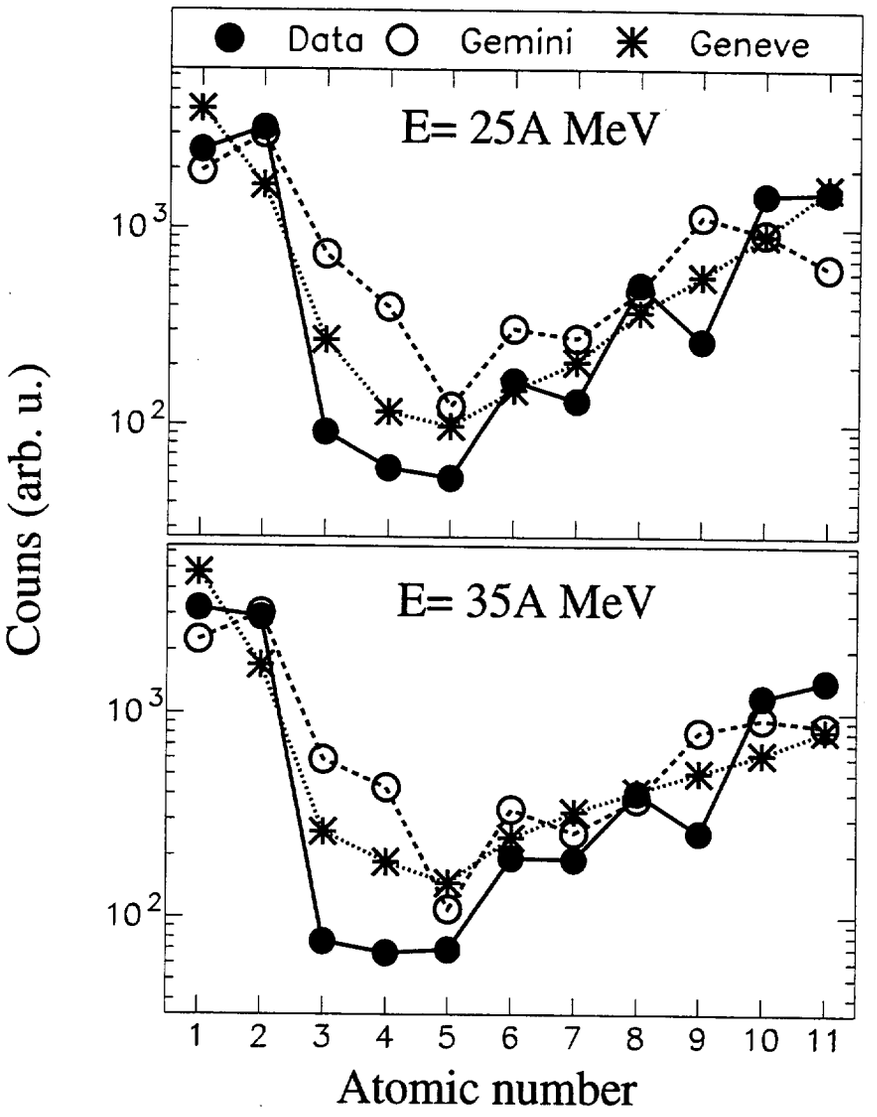

FIG. 2. M. Samri et al.

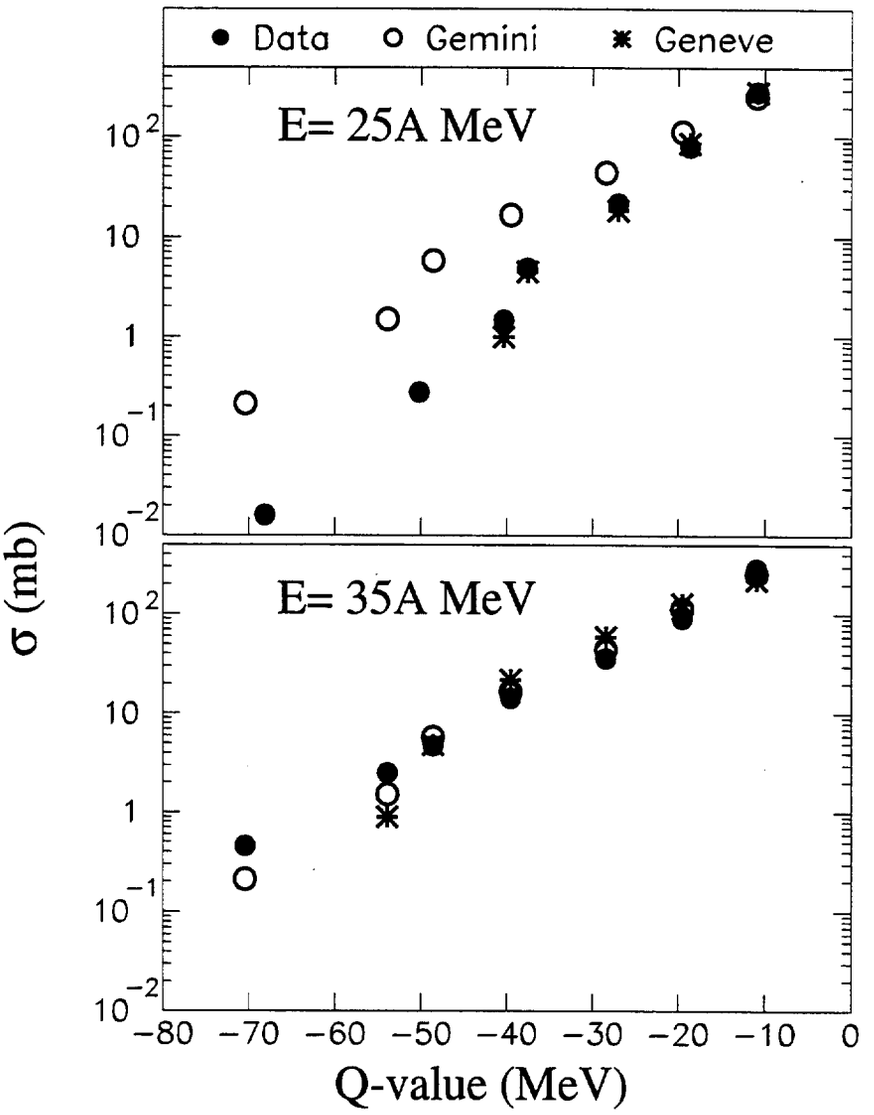

FIG. 3. M. Samri et al.

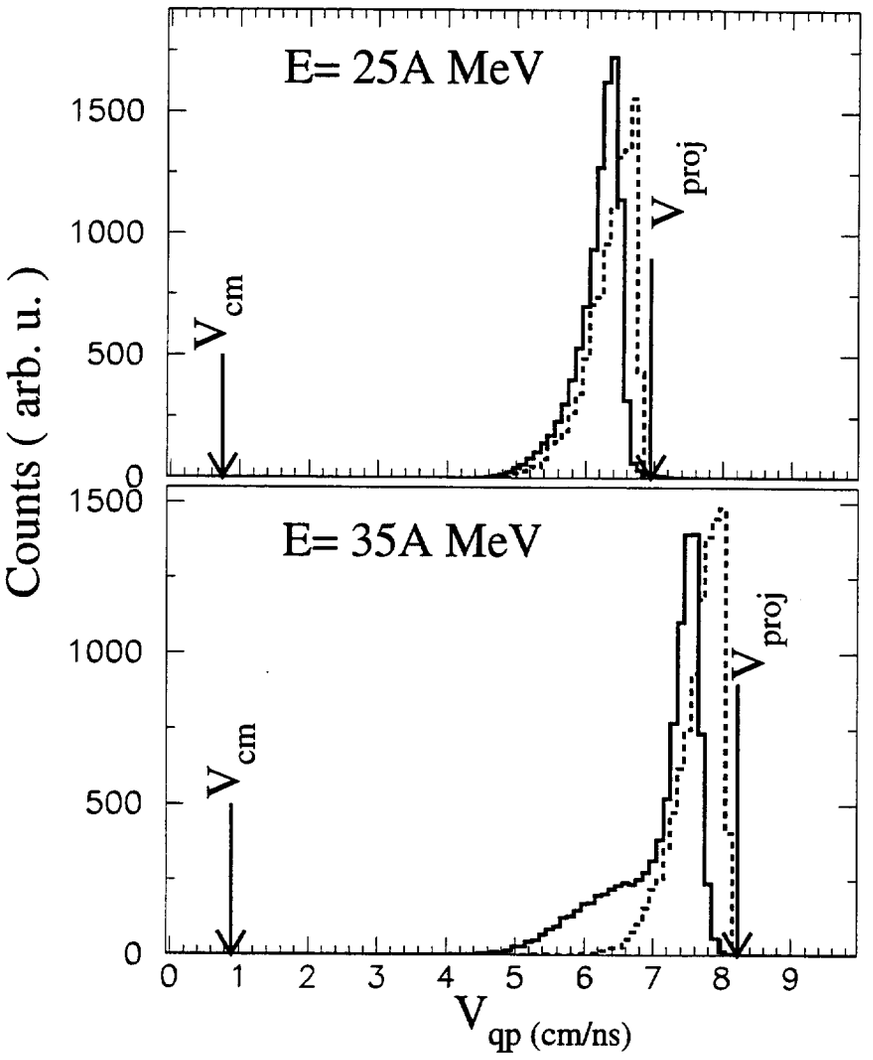

FIG. 4. M. Samri et al.

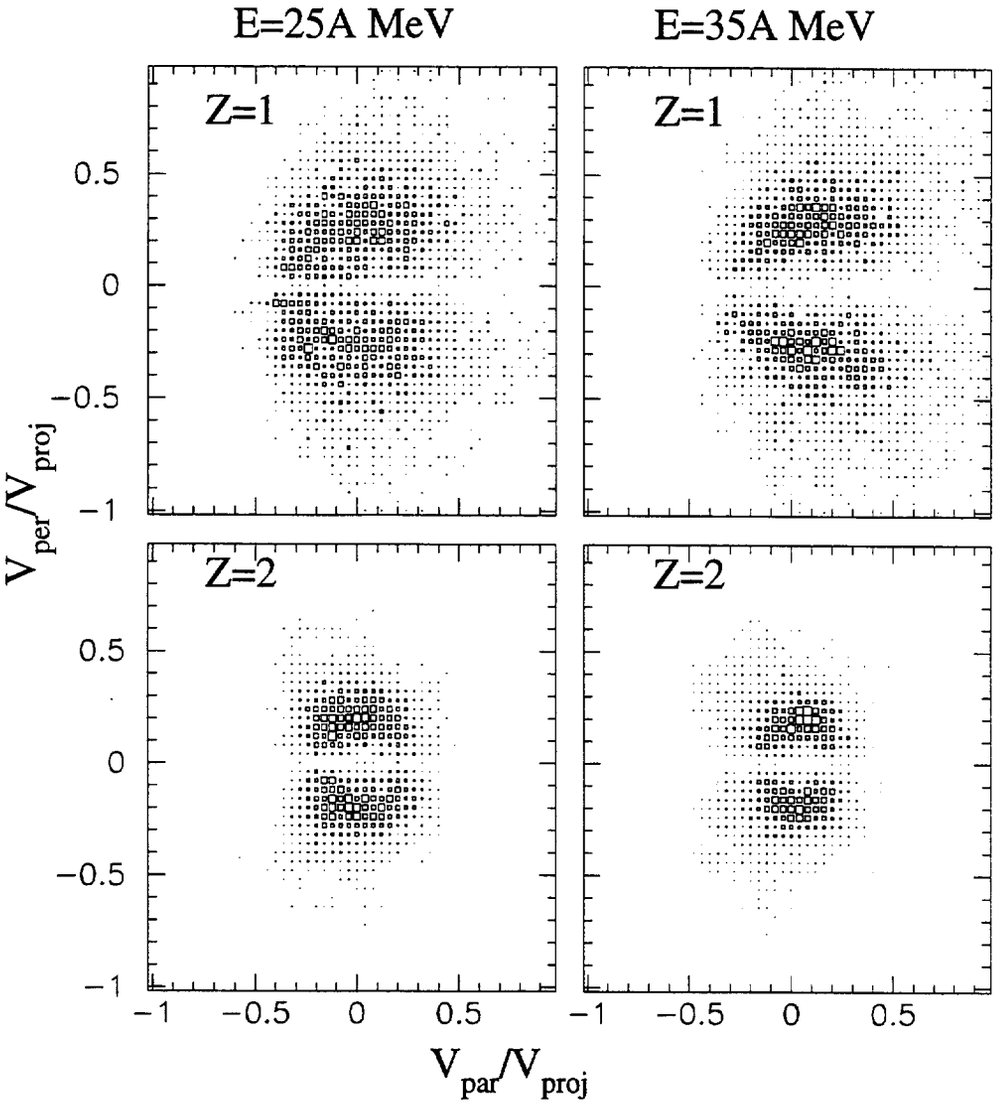

FIG. 5. M. Samri et al.

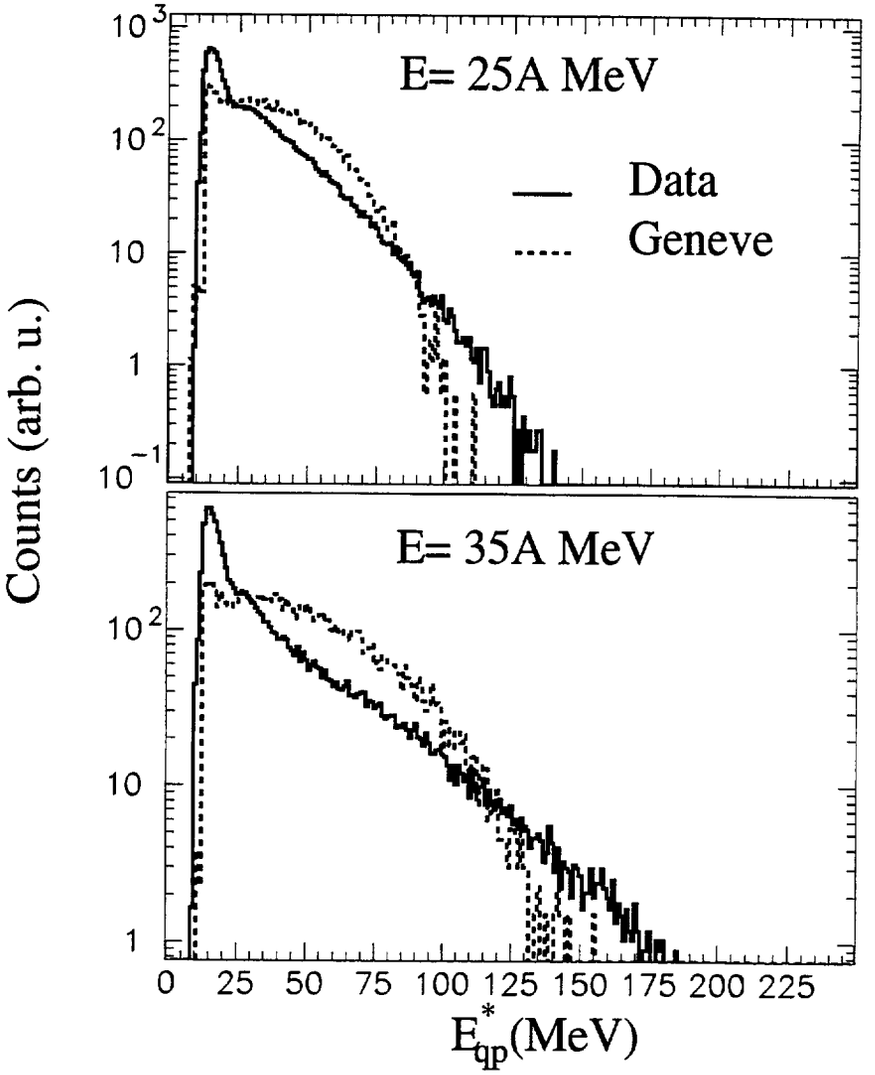

FIG. 6. M. Samri et al.

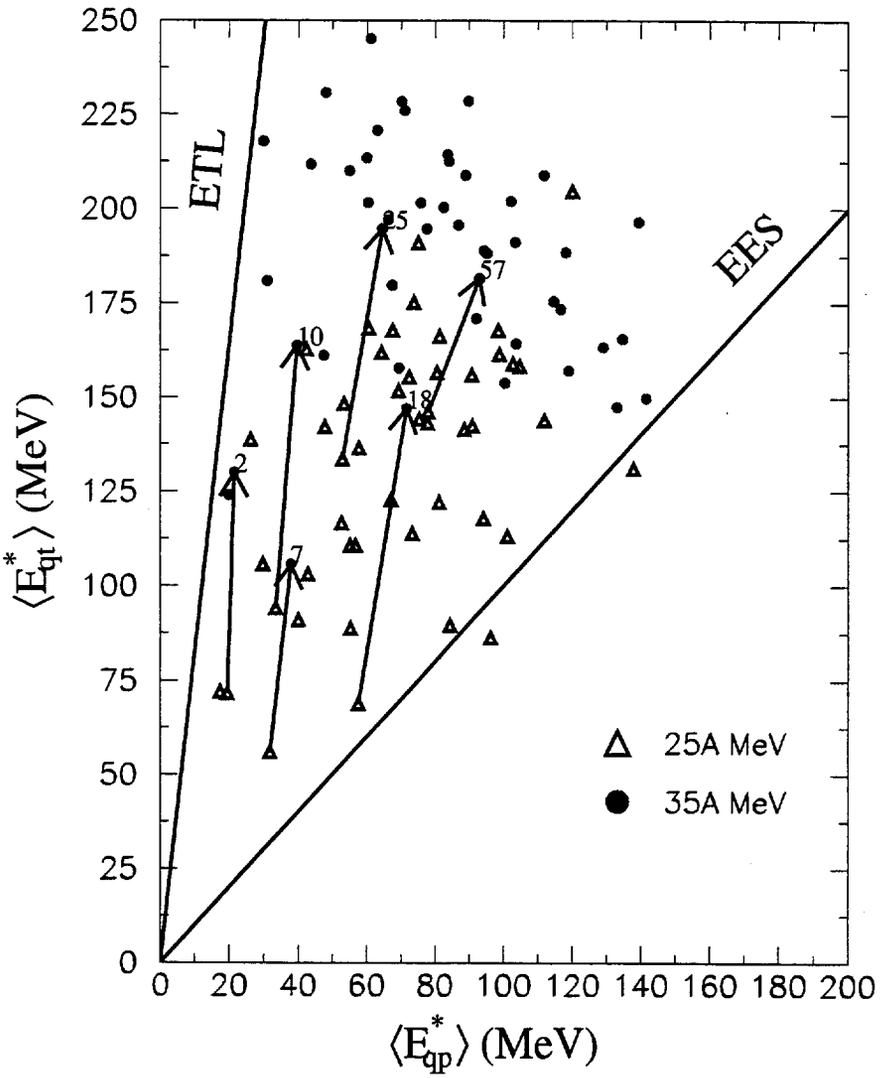

FIG. 7. M. Samri et al.

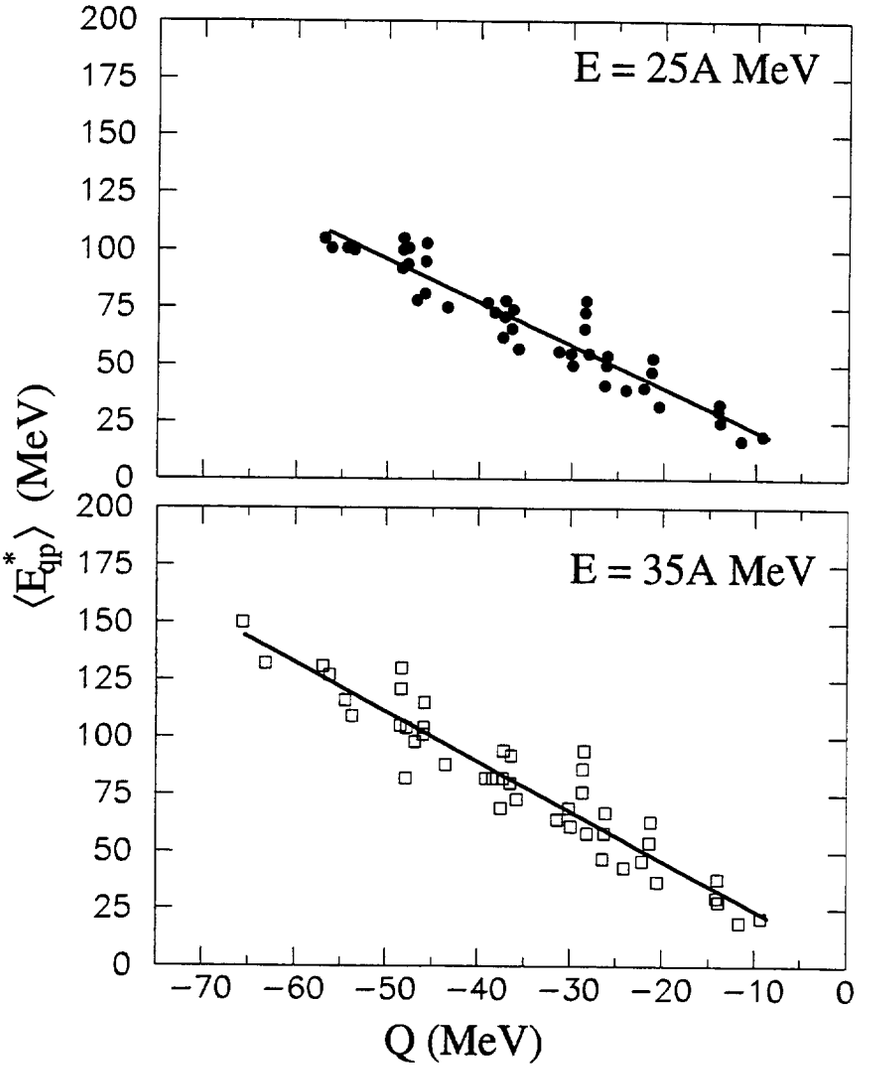

FIG. 8. M. Samri et al.

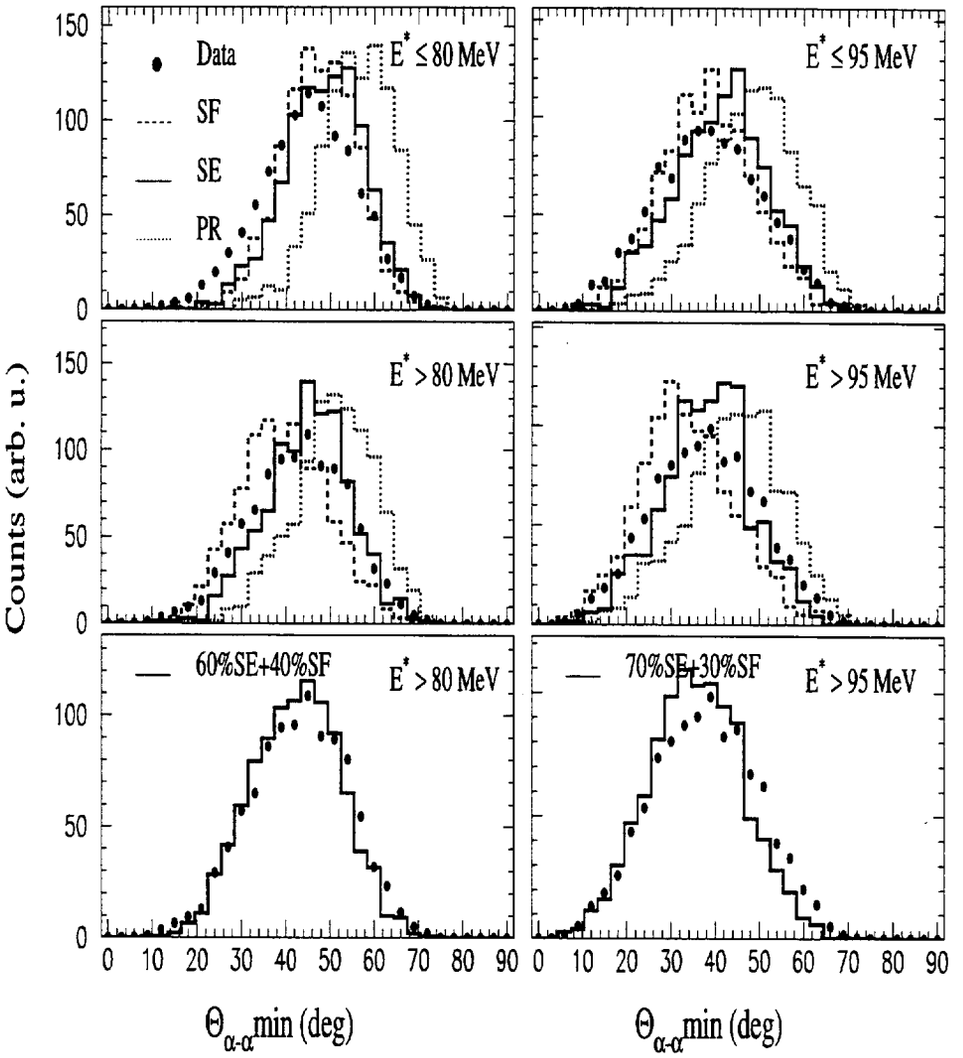

FIG. 9. M. Samri et al.

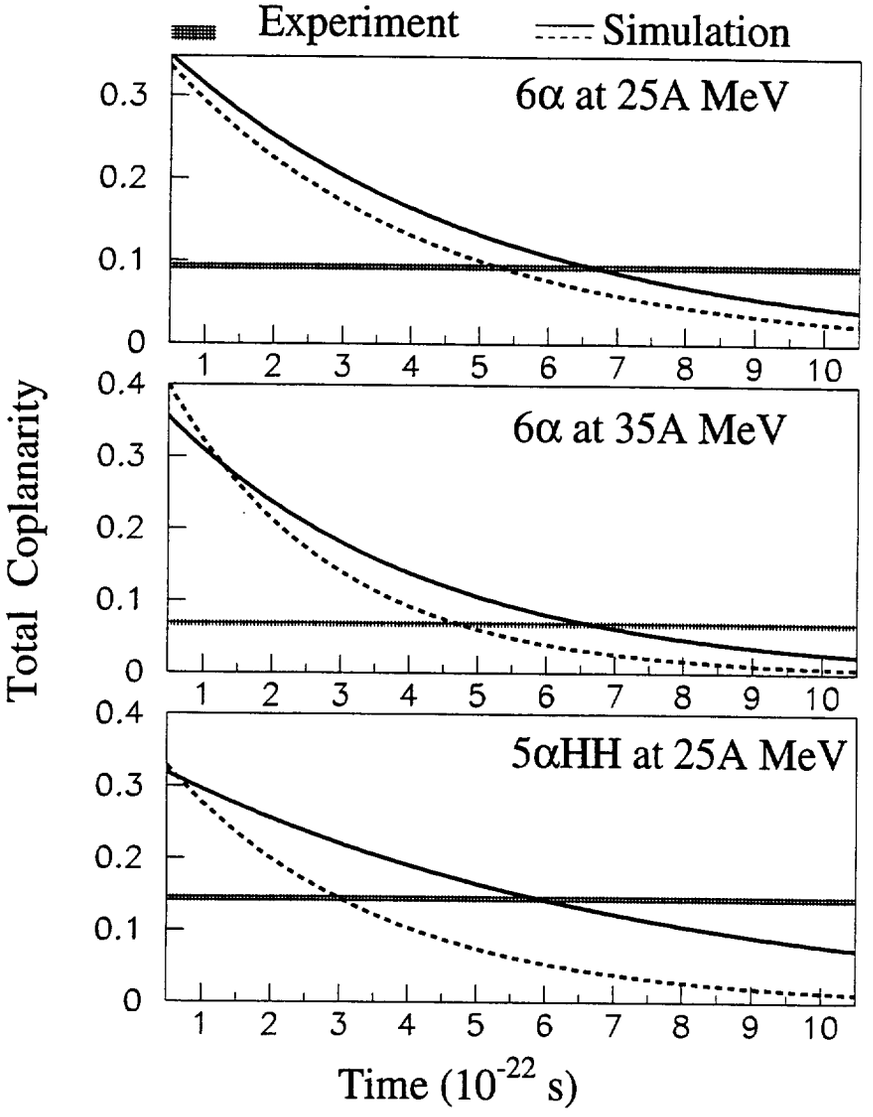

FIG. 10. M. Samri et al.